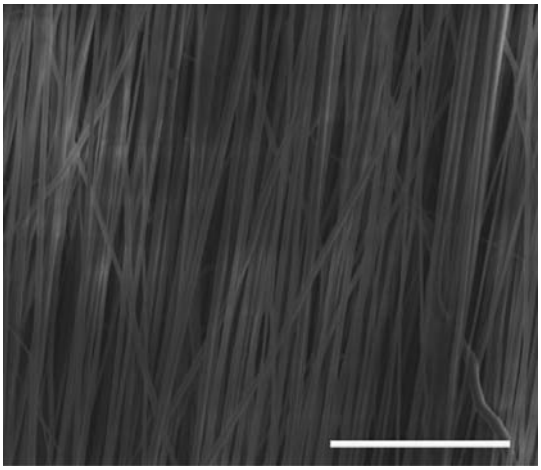

**Supplementary Figure S1 | High dense nanofibers array.** Prototypal SEM micrograph of high dense PVDF-TrFe nanofibers array. Scale bar: 10 μm.

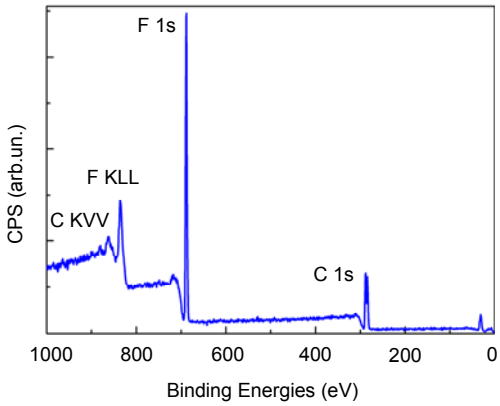


**Supplementary Figure S2 | XPS on nanofibers array**. XPS plot of PVDF-TrFe nanofibers array collected using a Kratos Axis ULTRA X-ray photoelectron spectrometer with monochromatic Al Kα excitation, 120 W (12kV, 10 mA).

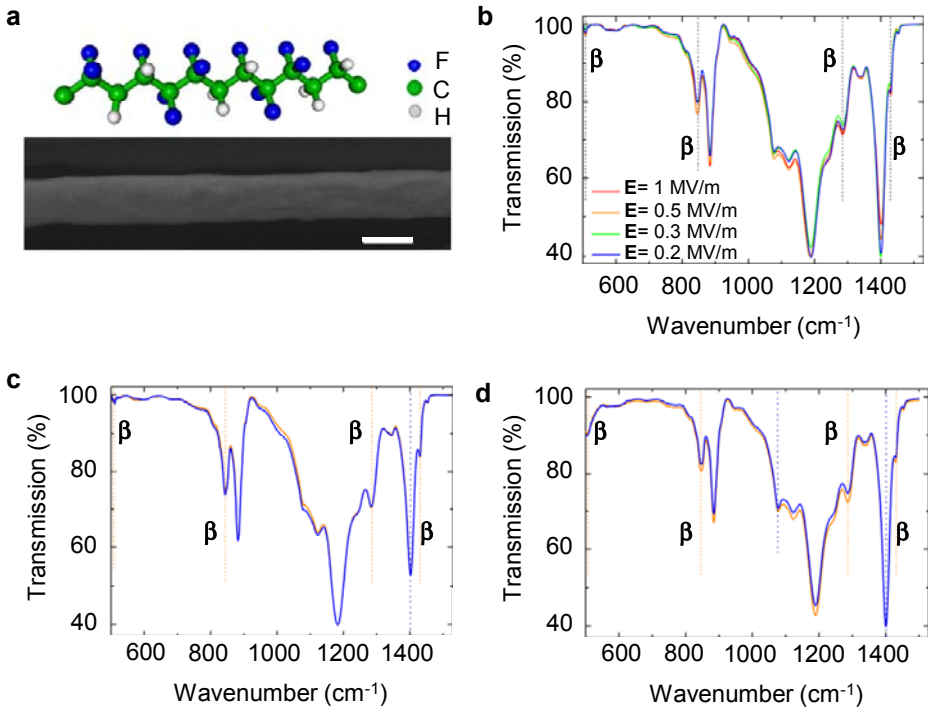


**Supplementary Figure S3 | Nanofibers array characterization.** (**a**) Schematics of chain conformation of P(VDF-TrFe) crystal β-phase in nanofibers array, according to FTIR and XRD analysis. The main molecular chains are preferentially aligned along the fiber longitudinal axis and the piezoelectric active dipoles (C-F) are perpendicular to the backbone direction. Bottom: SEM micrograph of a single P(VDF-TrFe) nanofiber. Scale bar 250 nm (**b**) FTIR spectra of aligned fiber array, produced by different electric field during electrospinning (0.2-1 MV/m). **c-d,** FTIR spectra measured under two mutually orthogonal incident beam polarization direction for films (**c**), and random fibers produced by 0.5 MV/m (**d**).

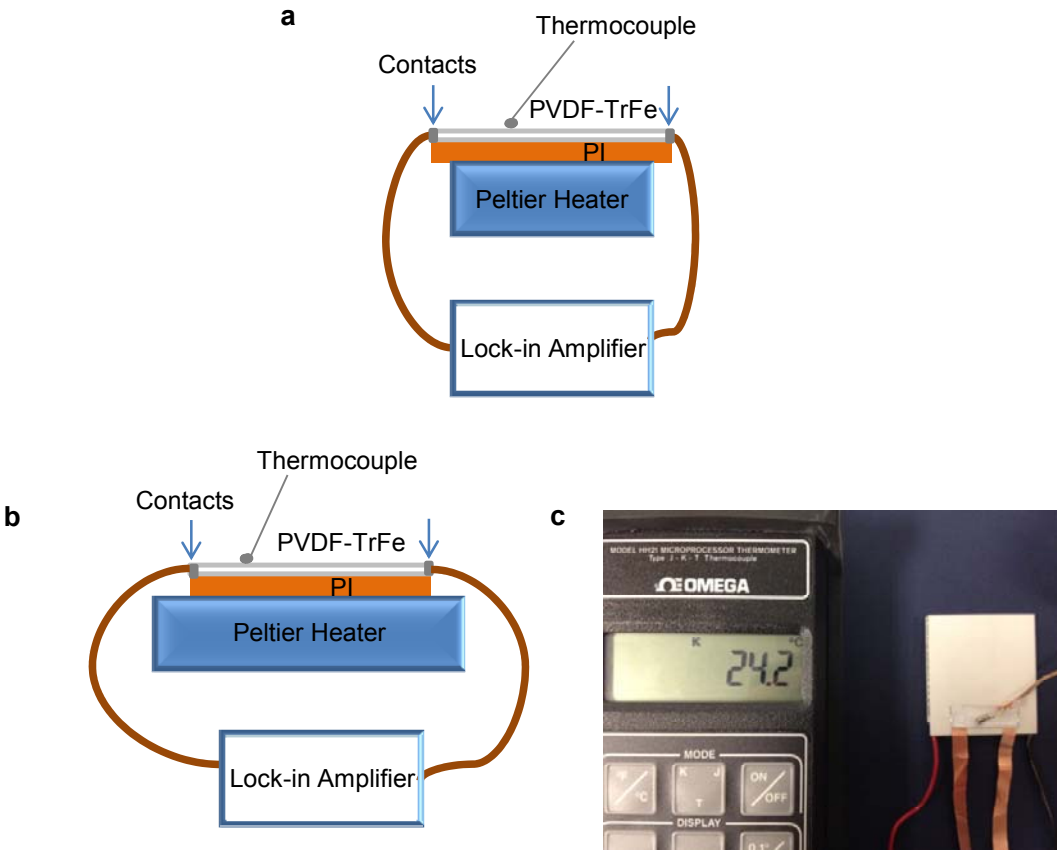


**Supplementary Figure S4 | Set-up used to measure pyroelectric signals.** Schematic illustration of the setup used to measure the pyroelectric signal with contacts positioned outside of (**a**) and on top of (**b**) the Peltier stage. (**c**) Image of temperature evaluation during a typical pyroelectric measurement.

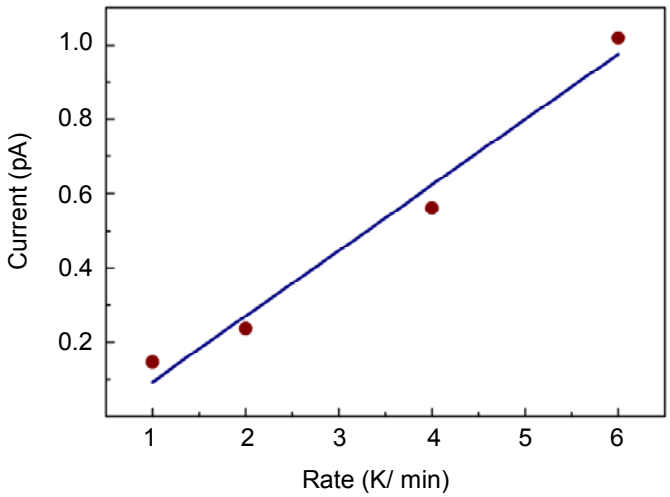


**Supplementary Figure S5 | Pyroelectric current.** Plot of the pyroelectric current as a function of rate of temperature change (dots) at a temperature of 20°C. The line corresponds to a linear fit.

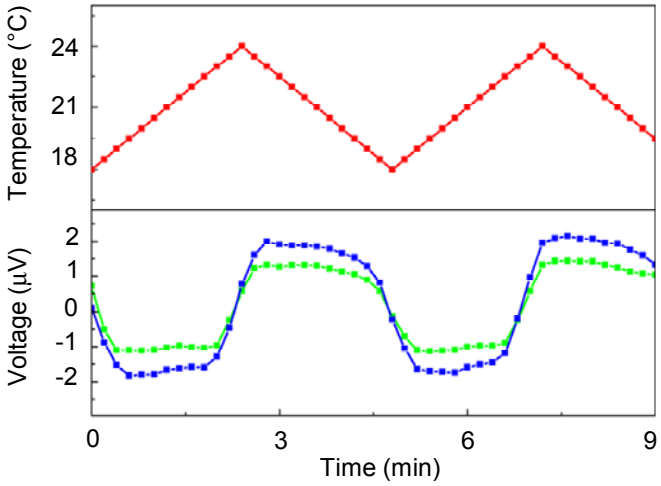


**Supplementary Figure S6 | Pyroelectric voltage.** Plot of the heating/cooling ramp applied to a nanofiber array device (red line) and the corresponding voltage recorded with contacts on top of (blue line) and outside of (green line) the Peltier stage.

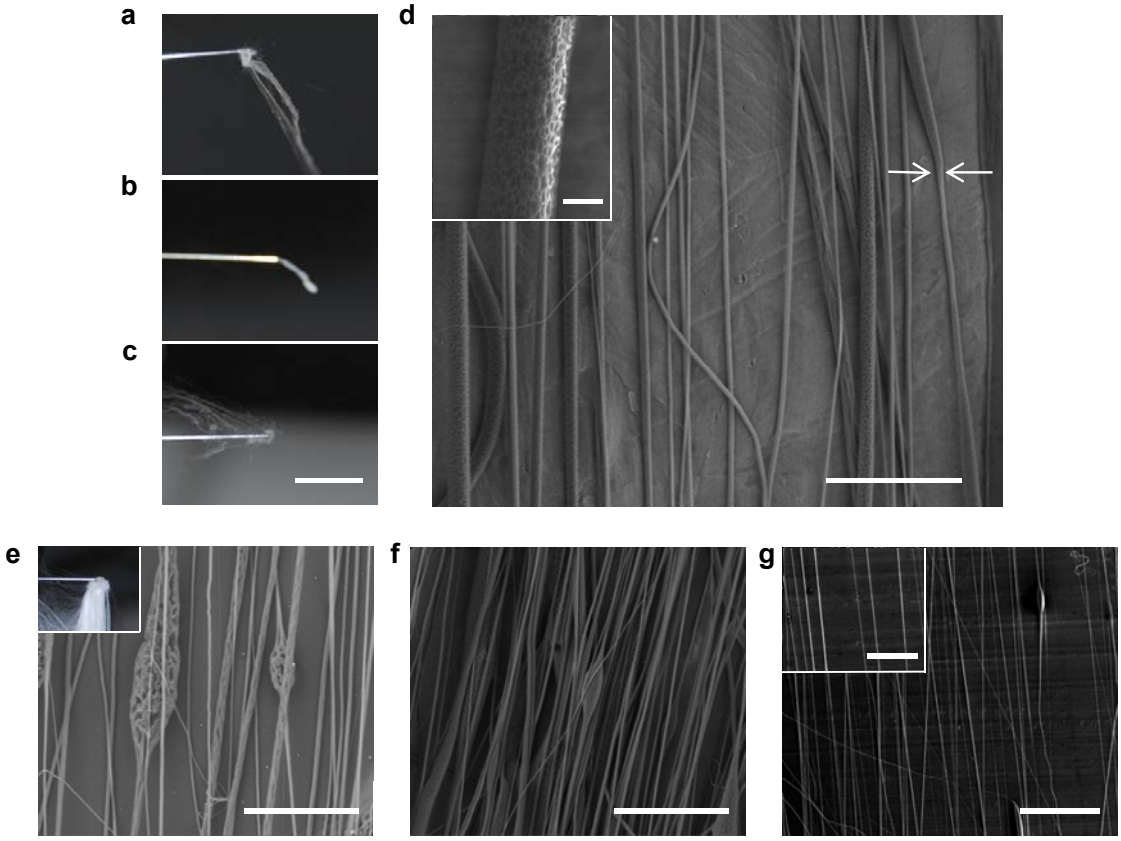


**Supplementary Figure S7 | Electrospinning experiments with low boiling solvents.** Photographs of needle clogging during electrospinning of PVDF-TrFe dissolved in Acetone (**a**), THF (**b**) and MEK (**c**) at a polymer/solvent concentration of 21% (w/w). Scale bar = 1 cm. (**d**) SEM micrograph of PVDF-TrFe fibers electrospun from a MEK solution (21%, w/w) prior to needle clogging. Arrows indicate an example of strong diameter variation along the fiber length. Scale bar 10 µm. Inset: magnified view of a single fiber to reveal the level of surface porosity . Scale bar 1 µm. (**e**) SEM micrograph of PVDF-TrFe fibers made by using ACE (12%, w/w). Scale bar 10 µm. Inset: photograph of needle clogged after 15 minutes of electrospinning. (**f**) SEM micrograph of PVDF-TrFe fibers made by using THF (12%, w/w). Scale bar 10 µm. (**g**) SEM micrograph of PVDF-TrFe fibers made by using MEK (17%, w/w). Scale bar 100 µm. Inset: Magnified SEM micrograph of the same sample. Scale bar: 40 µm.

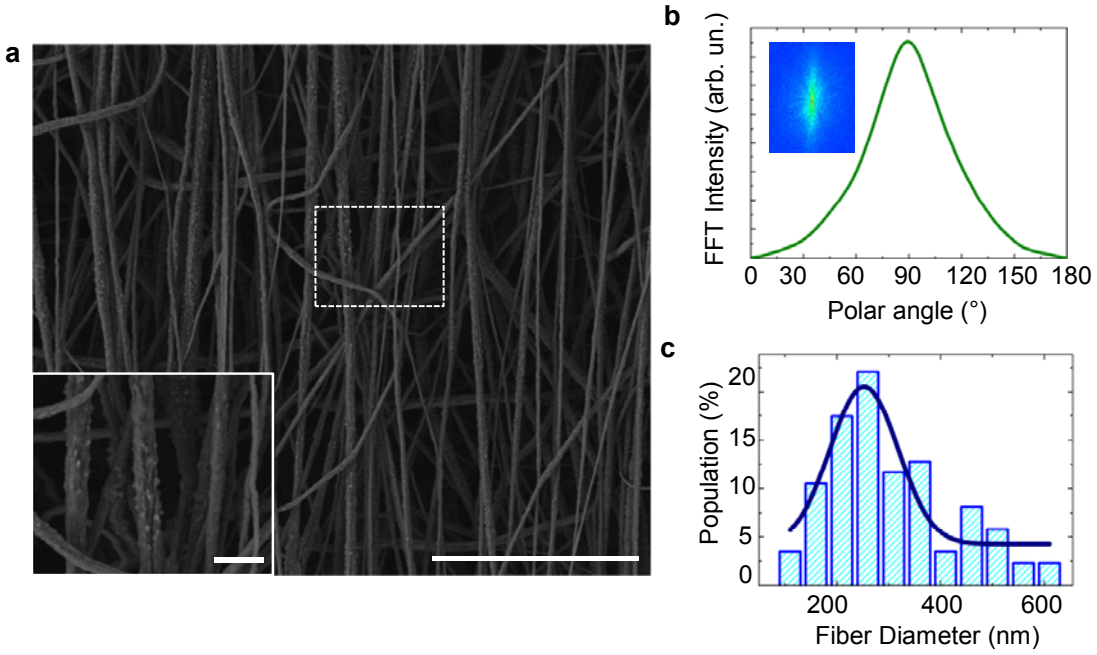


**Supplementary Figure S8 | Aligned array of PVDF nanofibers.** (**a**) SEM micrographs of PVDF fibers electrospun using the same experimental conditions as those for PVDF-TrFe. Scale bar: 10 μm. Inset: magnified view of the region indicated by a dashed square. Scale bar: 1 μm. (**b**) Radial intensity distribution vs detection angle (0-180°) for aligned arrays of PVDF fibers. The full width at half maximum is 51°. Inset: 2D FFT image. (**c**) Typical PVDF fiber diameter distribution and fit to a Gaussian shape (solid line).

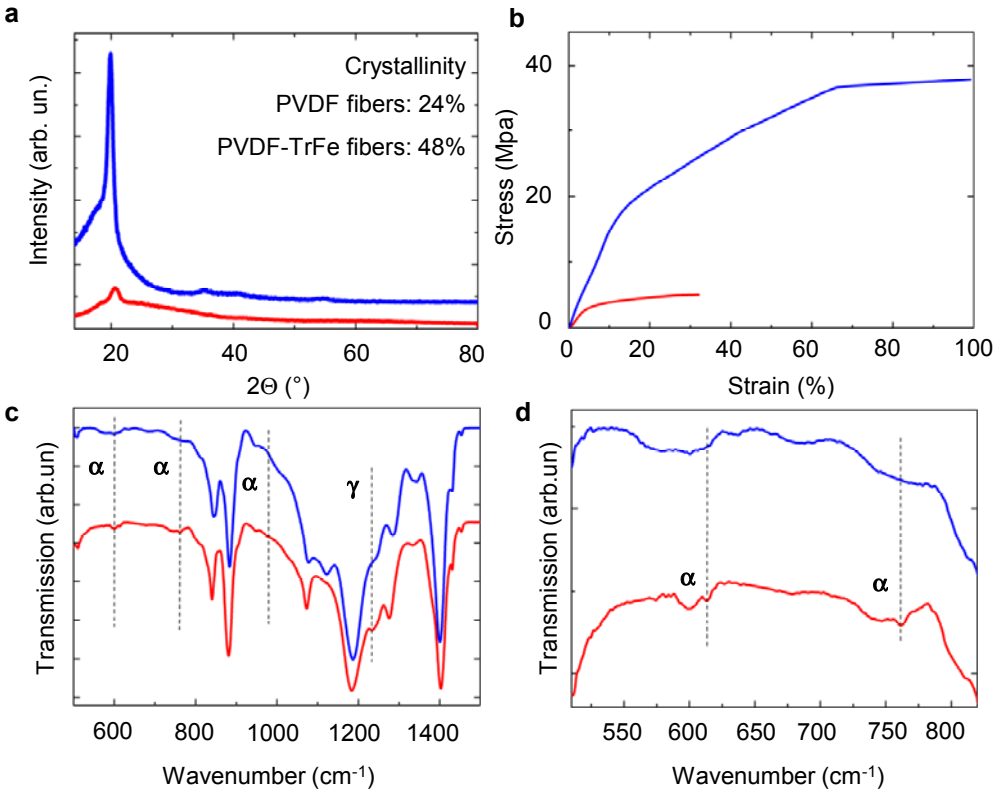


**Supplementary Figure S9 | Characterization of aligned arrays of PVDF nanofibers.** (**a**) X-ray diffraction patterns (XRD; Cu radiation with wavelength = 0.15418 nm) from aligned fibers of PVDF (red line) and PVDF-TrFE (blue line). The data are vertically shifted to facilitate comparison. (**b**)Typical stress-strain curves measured from aligned arrays of fibers of PVDF (red line) and PVDF-TrFe (blue line). (**c**) FTIR spectra of PVDF (red line) and PVDF-TrFe (blue line) aligned fibers. (**d**) Magnified view of the high energy region of the FTIR spectra, highlighting non-polar α bands at 612 and 762 $cm^{-1}$.

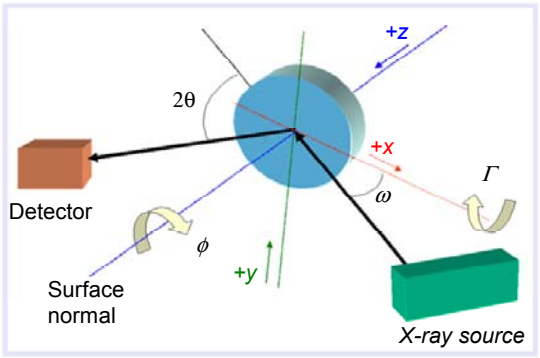


**Supplementary Figure S10 | Diagram of X-ray diffraction instrument.** X-ray analysis was carried out by performing 2θ/$\omega$ scans, where $\omega$ is the angle of incidence of X-ray beam relative to the sample surface and 2θ is the diffraction angle. The diffraction plane is defined by the incident and diffracted directions of the X-ray beams. Measurements performed at azimuthal rotation $\phi = 0$ where the fibers length parallel to the diffraction plane. $\Gamma$ indicate the tilt angle.

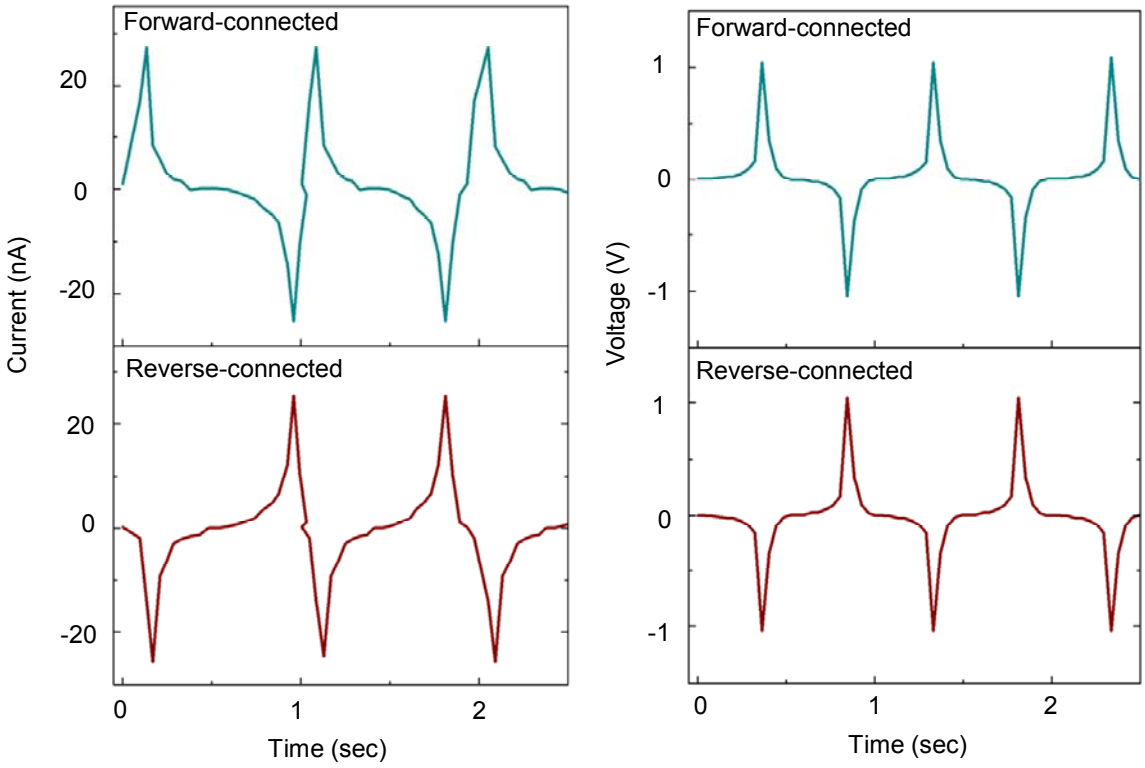


**Supplementary Figure S11 | Current and voltage measurements with reversed connections.** Short-circuit current and open circuit voltage measurements output of a typical nanofiber array device with forward (cyane blue line) and reversed (red wine line) connection to the measurement system. Connections showed reversal in signal polarity as expected.

**Supplementary Note 1. X-ray Photoelectron Spectra (XPS)**

X-ray photoelectron spectroscopy (XPS) is a quantitative spectroscopic technique that was used to calculate copolymerization ratio of PVDF-TrFE fiber array. XPS spectra were collected using a Kratos Axis ULTRA X-ray photoelectron spectrometer with monochromatic Al Kα excitation, 120 W (12kV, 10 mA). In order to reduce the effects of surface charging, the monochromatic source was operated using a bias voltage of 100 V. Data were collected using the low magnification (FOV1) lens setting with a 2 mm aperture (200 μm analysis area) and charge neutralizer settings of 2.1 A filament current, 2.1 V charge balance and 2 V filament bias. Survey spectra were collected at a pass energy of 160 eV and high resolution spectra were collected using a pass energy of 40 eV. The data were fitted with Gaussian-Lorentzian line shapes. The binding energy scale was referenced to the aliphatic C 1s line at 285.0 eV.

The copolymerization ratio was calculated by two different methods:

1) using Atomic concentrations calculated by curve fitting

Considering, the total % of Fluorine, % F= 16.03+36.73= 52.76 and that of Carbon,

% C= 2.39+17.22+6.43+20.44+0.77=47.25

The atomic ratio is $\frac{C}{F} = 0.90$ (i)

By taking into account the molecular formula of PVDF, $\left[\left(CH_2 - CF_2\right)_x\right]$ and TrFe, $\left[\left(CHF - CF_2\right)_{(1-x)}\right]$, the atomic ratio can be represented as,

$$\frac{C}{F} = \frac{2x + 2(1-x)}{2x + 3(1-x)} = \frac{2}{3-x} \quad \text{(ii)}$$

Equaling (i) and (ii),

$$\frac{C}{F} = 0.90 = \frac{2}{3-x}$$

Therefore, the fraction of PVDF, x= 0.78 and the fraction of TrFe, 1-x = 0.22

2) using peak area ratios calculated by using C1s curve fitting:

| Characteristic Peak | DOS (BE) | Area % | Normalized to 100% |
|---|---|---|---|
| PVDF | 286.7 | 36.45 | 72.81 |
| TrFE | 289.0 | 13.61 | 27.17 |

The fraction of PVDF equals to 0.73, while the fraction of TrFe is 0.27

From the XPS spectra, the stoichiometric ratio (in atomic percent) of two elements, C and F, in the P(VDF–TrFe) film is determined. Co-polymerization ratio of PVDF:TrFe (0.73:0.27) from

XPS results shows excellent agreement with actual co-polymer ratio of commercial PVDF:TrFE (0.75:0.25).

**Supplementary Note 2. Piezoelectric analysis of PVDF-TrFe fiber arrays under compression**

The constitutive model of piezoelectric materials gives the relations among the stress $\sigma_{ij}$, strain $\varepsilon_{ij}$, electric field $E_i$ and electric displacement $D_i$ as

$$\begin{Bmatrix}\sigma_{11}\\ \sigma_{22}\\ \sigma_{33}\\ \sigma_{23}\\ \sigma_{31}\\ \sigma_{12}\end{Bmatrix}=\begin{bmatrix}c_{11} & c_{12} & c_{13} & 0 & 0 & 0\\ c_{12} & c_{11} & c_{13} & 0 & 0 & 0\\ c_{13} & c_{13} & c_{33} & 0 & 0 & 0\\ 0 & 0 & 0 & c_{44} & 0 & 0\\ 0 & 0 & 0 & 0 & c_{44} & 0\\ 0 & 0 & 0 & 0 & 0 & (c_{11}-c_{12})/2\end{bmatrix}\begin{Bmatrix}\varepsilon_{11}\\ \varepsilon_{22}\\ \varepsilon_{33}\\ 2\varepsilon_{23}\\ 2\varepsilon_{31}\\ 2\varepsilon_{12}\end{Bmatrix}-\begin{bmatrix}0 & 0 & e_{31}\\ 0 & 0 & e_{31}\\ 0 & 0 & e_{33}\\ 0 & e_{15} & 0\\ e_{15} & 0 & 0\\ 0 & 0 & 0\end{bmatrix}\begin{Bmatrix}E_1\\ E_2\\ E_3\end{Bmatrix}, \tag{S1}$$

$$\begin{Bmatrix}D_1\\ D_2\\ D_3\end{Bmatrix}=\begin{bmatrix}0 & 0 & 0 & 0 & e_{15} & 0\\ 0 & 0 & 0 & e_{15} & 0 & 0\\ e_{31} & e_{31} & e_{33} & 0 & 0 & 0\end{bmatrix}\begin{Bmatrix}\varepsilon_{11}\\ \varepsilon_{22}\\ \varepsilon_{33}\\ 2\varepsilon_{23}\\ 2\varepsilon_{31}\\ 2\varepsilon_{12}\end{Bmatrix}+\begin{bmatrix}k_{11} & 0 & 0\\ 0 & k_{22} & 0\\ 0 & 0 & k_{33}\end{bmatrix}\begin{Bmatrix}E_1\\ E_2\\ E_3\end{Bmatrix}. \tag{S2}$$

Consider a uniaxial compression applied along the $x_1$ direction (normal to fibers, Fig. 3a) instantaneously at time $t$=0, i.e., i.e., $\sigma_{11}=-pH(t)$, where $H$ is the Heavyside step function $H(t)=\begin{cases}0 & for \quad t<0\\ 1 & for \quad t\geq 0\end{cases}$. For $\varepsilon_{22}=\varepsilon_{33}\approx 0$ because the P(VDF-TrFE) fiber arrays (elastic modulus ~ 200 MPa) are bonded to the much thicker and stiffer plastic substrate (elastic modulus 2.5 GPa), Eqs. (S1) and (S2) give $-pH(t)=c_{11}\varepsilon_{11}-e_{31}E_3$ and $D_3=e_{31}\varepsilon_{11}+k_{33}E_3$, respectively, where $D_3$ is the electric displacement along the poling direction, and the electric field $E_3$ is related to the voltage $V$ and effective contact length $L_{eff}$ by $E_3=V/L_{eff}$. Elimination of $\varepsilon_{11}$ from these two equations yields the electric displacement $D_3=-\bar{d}pH(t)+(\bar{k}V/L_{eff})$, where $\bar{d}=e_{31}/c_{11}$ and $\bar{k}=k_{33}+e_{31}^2/c_{11}$. The voltage $V$ and current $I=-h_{PVDF-TrFe}w_{PVDF-TrFe}\dot{D}_3$ are also related by the resistance $R$ of the voltmeter, $V$=$IR$. These yield the coupling equation of the voltage

$$\frac{dV}{dt}+\frac{L_{eff}}{\bar{k}h_{PVDF-TrFe}w_{PVDF-TrFe}R}V=\frac{\bar{d}L_{eff}}{\bar{k}}\delta(t), \tag{S3}$$

where $\delta(t)$ is the delta function. For the initial condition $V(t=0^-)=0$, the solution of Eq. (S3) is $V=(\bar{d}L_{eff}/\bar{k})\,p\exp\left[-L_{eff}t/(\bar{k}Rh_{PVDF-TrFe}w_{PVDF-TrFe})\right]$. The maximum value is given in Eq. (1) in the main text.

**Supplementary Note 3. Piezoelectric analysis of PVDF-TrFe fiber arrays under bending**

**3.1 Mechanics analysis**

For the out-of-plane displacement $w = A\left[1+\cos\left(2\pi x_3/L_{PI}\right)\right]/2$ in plane-strain analysis ($\varepsilon_{22}=0$), the bending energy in flexible polymide support (PI) is $\left(EI/2\right)\int\left(w''\right)^2 ds$, where $w''$ and $EI$ are the curvature and plane-strain bending stiffness of PI substrate, respectively, and the integration is over the length of PI substrate. The membrane energy can be obtained following the same approach of Song et al. [39] Minimization of total energy (sum of bending and membrane energies) gives the amplitude $A$ as

$$A = \frac{2}{\pi}\sqrt{L_{PI}\cdot\Delta L - \frac{\pi^2 t_{PI}^2}{3}} \approx \frac{2}{\pi}\sqrt{L_{PI}\cdot\Delta L}\,, \tag{S4}$$

where the last approximation holds when the compression of PI substrate $\Delta L \approx t_{PI}^2/L_{PI}$ as in the experiment. The strain in the fiber arrays is obtained from the curvature and the distance between the mid-planes of PI substrate and fiber arrays as

$$\varepsilon_{33} = \frac{\pi^2\left(h_{PI}+h_{PVDF-TrFe}\right)A}{L_{PI}^2}\cos\left(\frac{2\pi x_3}{L_{PI}}\right). \tag{S5}$$

The pure bending of PI substrate, together with the traction-free condition on the surface of the fiber arrays, gives $\sigma_{11}=0$ in the fiber arrays. Its substitution into Eq. (S1) yields $\varepsilon_{11} = -\left(c_{13}/c_{11}\right)\varepsilon_{33} + \left(e_{31}/c_{11}\right)E_3$. The electric field $E_3$ is then obtained from Eq. (S2) as

$$E_3 = -\frac{\overline{e}}{\overline{k}}\varepsilon_{33} + \frac{1}{\overline{k}}D_3\,, \tag{S6}$$

where the electric displacement $D_3$ is spatially invariant (established from the charge equation $dD_3/dx_3=0$) and is to be determined.

**3.2 Current**

The voltage across the length of the fiber arrays $L_{PVD\text{-}TreF}$ is zero, $\int_{-L_{PVDF-TrFe}/2}^{L_{PVDF-TrFe}/2} E_3 dx_3 = 0$, after the fiber arrays is connected to an ampere meter. Together with Eqs. (S5) and (S6), it gives the electric displacement

$$D_3 = \frac{2\bar{e}\left(h_{PI} + h_{PVDF-TrFe}\right)}{L_{PVDF-TrFe}} \sqrt{\frac{\Delta L}{L_{PI}}} \sin\left(\pi \frac{L_{PVDF-TrFe}}{L_{PI}}\right). \quad \text{(S7)}$$

The electric charge is the product of $-D_3$ and the cross section area $h_{PVDF\text{-}TrFe} w_{PVDF\text{-}TrFe}$ of the fiber arrays. Its rate of change gives the current

$$I = -\frac{\bar{e}\left(h_{PI} + h_{PVDF-TrFe}\right) h_{PVDF-TrFe} w_{PVDF-TrFe}}{L_{PVDF-TrFe}\sqrt{L_{PI}\Delta L}} \frac{d\Delta L}{dt} \sin\left(\pi \frac{L_{PVDF-TrFe}}{L_{PI}}\right). \quad \text{(S8)}$$

For the representative $\Delta L$ in the main text, the maximum current in Eq. (2) is obtained.

### 3.3 Voltage

Let $V$ denote the voltage across the length of the fiber arrays $L_{PVDF\text{-}TrFe}$ after the fiber arrays is connected to a voltmeter. This requires $\int_{-L_{PVDF-TrFe}/2}^{L_{PVDF-TrFe}/2} E_3 dx_3 = V$, which, together with Eqs. (S5) and (S6), gives the electric displacement

$$D_3 = \frac{2\bar{e}\left(h_{PI} + h_{PVDF-TrFe}\right)}{L_{PVDF-TrFe}} \sqrt{\frac{\Delta L}{L_{PI}}} \sin\left(\pi \frac{L_{PVDF-TrFe}}{L_{PI}}\right) + \frac{\bar{k}}{L_{PVDF-TrFe}} V. \quad \text{(S9)}$$

Similar to Supplementary Note 3.2, the rate of change of Eq. (S9) gives the current

$$I = -\frac{\bar{e}\left(h_{PI} + h_{PVDF}\right) h_{PVDF-TrFe} w_{PVDF-TrFe}}{L_{PVDF-TrFe}\sqrt{L_{PI}\Delta L}} \frac{d\Delta L}{dt} \sin\left(\pi \frac{L_{PVDF-TrFe}}{L_{PI}}\right) - \frac{\bar{k} h_{PVDF-TrFe} w_{PVDF-TrFe}}{L_{PVDF-TrFe}} \frac{dV}{dt}. \quad \text{(S10)}$$

Its relation with the resistance $R$ of the voltmeter leads to Eq. (3) and the maximum voltage in Eq. (4).

**Supplementary Note 4. Pyroelectric measurements**

Pyroelectric effects were investigated by measuring both the current and voltage output of a nanofiber array device using the continuous heating/cooling method at zero dc voltage and at a constant heating/cooling rate between 1 to 6 K/min. A small stage (All Electronics Corp.; 40x44 mm, which closely matches the lengths of the fibers) was used to investigate effects of temperature on just the fiber region of the device as shown in Figure S4a. We also used a slightly larger stage (Monster; 62x62 mm) as shown in Figure S4b to examine the effects of temperature on the entire device, including the electrode contacts. The heating rates and temperature ranges correspond, roughly, to those in references 40, 41, 42. Figure S4 provides a schematic illustration of the setups. Throughout the experiments, the sample temperature was measured with a NiAl thermocouple and a Model HH21 Omega microprocessor thermometer. The pyroelectric coefficient can be measured by the Lang-Steckel method[41]. The governing equation for the pyroelectric effect is

$$D_3 = \alpha T + k_{33} E_3, \tag{S11}$$

where $\alpha$ is the pyroelectric coefficient, and $T$ is the change of the temperature. For current measurements using an ammeter, the voltage across the fiber length, and therefore the electric field $E_3$, are zero such that $D_3 = \alpha T$. The rate of the change in temperature creates a current given by $I(t) = -\alpha h_{PVDF-TrFe} w_{PVDF-TrFe}\, dT/dt$, which can be used to measure the pyroelectric coefficient as

$$\alpha = -\frac{I(t)}{h_{PVDF-TrFe} w_{PVDF-TrFe}\, dT/dt}. \tag{S12}$$

For the measurement results in Figure S5 $I(t)/(dT/dt) = 10.9\ pC/K$, and $h_{PVDF\text{-}TrFe}$=20 μm and $w_{PVDF\text{-}TrFe}$= 8 mm, Eq. (S12) gives the pyroelectric coefficient as $\alpha$=-68 μC/(m$^2$K), which is in the same range as values reported for thin films of PVDF-TrFe films (-20μC/m$^2$K) [42]. At a constant heating rate of 2.5 K/min, the pyroelectric signals follow the derivative of the temperature, with maximum voltages of 1.9 mV and 1.3 mV when contacts are on top of and outside of the heater, respectively. The responses are symmetrical with respect to heating and cooling, as expected. The magnitudes of these voltages are nearly 50 times smaller than the smallest piezovoltages reported in the manuscript (i.e. those that result from tests at 0.1 Pa). The corresponding pyroelectric analysis is reported in Supplementary Note 5.

**Supplementary Note 5. Pyroelectric analysis**

For voltage measurement of the fiber arrays via a voltmeter, Eq. (S11) still holds. The electric field $E_3$ and electric displacement $D_3$ are related to the voltage $V$ and current $I$ by $E_3 = V/L_{PVDF-TrFe}$ and $I = -h_{PVDF-TrFe} w_{PVDF-TrFe} \dot{D}_3$, respectively, where $L_{PVDF-TrFe}$ is the length of fiber arrays and $h_{PVDF-TrFe} w_{PVDF-TrFe}$ is the cross section area. The voltage $V$ and current $I$ are also related by the resistance $R$ of the voltmeter, $V=IR$. These give the equation for V as

$$\frac{dV}{dt} + \frac{L_{PVDF-TrFe}}{k_{33} R h_{PVDF-TrFe} w_{PVDF-TrFe}} V = -\frac{\alpha L_{PVDF-TrFe}}{k_{33}} \frac{dT}{dt}. \quad \text{(S16)}$$

For the initial condition $V(t=0)=0$, the above equation has the solution

$$V = -\frac{\alpha L_{PVDF-TrFe}}{k_{33}} \int_0^t \frac{dT}{d\tau} e^{\frac{L_{PVDF-TrFe}}{k_{33} R h_{PVDF-TrFe} w_{PVDF-TrFe}} (\tau - t)} d\tau. \quad \text{(S17)}$$

For $L_{PVDF\text{-}TrFe}$=40 mm, thickness $h_{PVDF}$=20 μm, width $w_{PVDF\text{-}TrFe}$=8 mm, and the measured pyroelectric coefficient $\alpha = -68$ μC/(m$^2$K) and resistance of the voltmeter $R$=4 MΩ in experiments, the maximum voltage is 1.81 μV for the measured temperature $T(t)$ in Fig. S6 and the dielectric constant $k_{33}$=5.31*10$^{-11}$ F/m [38]. In fact, for the normalized time $L_{PVDF-TrFe} t/(S k_{33} R) \gg 1$, Eq. (S17) can be simplified to Eq. (5) in the main text, which also gives the maximum voltage 1.81 V, and agrees well with maximum voltage of 1.9 V when the PVDF-TrFe fiber arrays are in contact with the top of the heater.

It should be pointed out that different voltmeters were used for pyroelectric and piezoelectric measurements, with resistance of the voltmeter R=4 MΩ and 70 MΩ, respectively due to different sensing range of voltmeters. Even for R=70 MΩ and heating rate 6.5 K/min, the pyroelectric voltage is still smaller than the piezoelectric voltage even at the lower end of the range of pressure sensitivity (0.1 Pa, in the type of tests reported here).

**Supplementary Note 6. Comparison between PVDF-TrFe and PVDF fibers**

For purposes of comparison, PVDF fibers were formed with the same experimental conditions used for PVDF-TrFe. In particular, PVDF (Sigma Aldrich) was dissolved in a 3:2 volume ratio of dimethylformamide/acetone at a polymer/solvent concentration of 21% w/w. A potential of 30 kV was applied between a nozzle tip with inner diameter of 200 μm, fed by a syringe pump at a flow-rate of 1 mL/hr, and a collector at a distance of 6 cm. The collector disk rotated at angular speed of 4000 rpm, corresponding to linear speeds > 16 m/s at the collector surface. The fibers were collected on aluminium strips with widths of 0.8 cm and lengths of 25 cm. The morphological, crystallographic and mechanical properties of PVDF fibers were measured and compared with those of PVDF-TrFe. The most immediate, striking difference from PVDF-TrFe was that the PVDF fibers were not sufficiently robust to exist as stable, free-standing films. In nearly all cases the process of detaching the PVDF fibers from the aluminium foil mechanically destroyed the samples by fracture and tearing. Furthermore, we found that PVDF fibers are poorly aligned (Figure S8a). 2D FFT analysis indicates that the full width at half maximum of the radial intensity distribution of the elliptical profile is 51°, which is more than three times larger than that of the PVDF-TrFe arrays (Figure S8b). Although the average fiber diameters (250 nm) and the corresponding distribution of diameters are comparable (Figure S8c), the surfaces of the PVDF fibers are rough, with protrusions that have characteristic dimensions of ~100 nm (Inset of Figure S9a). X-ray diffraction (XRD) patterns indicate that PVDF fibers exhibit 24% crystallinity, which is two times lower than that of PVDF-TrFe fibers (Figure S9a) and the non-polar $\alpha$ (612,762, 976 $cm^{-1}$) and $\gamma$ (1234 $cm^{-1}$) phases are here clearly distinguishable by FTIR (Figure S9c and d). The mechanical properties were investigated using dynamic mechanical analysis (DMA Q800, TA Instruments, New Castle, DE), in tensile mode at constant temperature (25°C). At least three different fibrous specimens for each polymer were tested. Specimen dimensions were approximately 8.0×12.0 mm (width×length) with thicknesses between 20 and 40 μm. The stress-strain curves were recorded with a ramp/rate of 0.5 N/min (up to 18 N). Typical stress-strain curves of PVDF and PVDF-TrFe fibers are reported in Figure S9b. The measured Young Modulus is 168 ±8 MPa for PVDF-TrFe and 86 ±11 MPa for PDVF fibers respectively. The maximum elongation of PVDF-TrFE fibers is ~100% (corresponding to a tensile strength of about 40 MPa) while that of PVDF fibers is ~32% (corresponding to a tensile strength of about 5 MPa). These results clearly indicate that PVDF-TrFe fibers exhibit superior mechanical properties compared to PVDF fibers. Such differences are critically important to use in the classes of devices described in our manuscript. In addition, the formation of inter-fibers joints or adhesion points further increase both the tensile strength and the elongation path[44].

**Supplementary Methods . PVDF-TrFe fibers made with low-boiling solvents**

PVDF-TrFe was dissolved in three different low-boiling point ($T_b$) solvents: Acetone (ACE, $T_b$: 57°C), Tetrahydrofuran (THF, $T_b$: 66°C) and methylethylketone (MEK, $T_b$: 80°C) at different polymer/solvent concentrations in the range 12-21% (w/w). At the highest concentration, needle clogging occurs almost instantaneously with ACE and THF (Figure S7 a and b respectively), and after tens of seconds with MEK (Figure S7c). In this last case, collected fibers take the form of isolated strands (about 7 $x10^2$ roughly parallel fibers per mm) with an average diameter ~570 nm. Such fibers have non-uniform morphologies, with both flat and porous surfaces, and in short, discontinuous segments due to the presence of necks and beads (Figure S7d).

At lower concentrations, the maximum electrospinning time could be extended to ~15 minutes with ACE (corresponding to 300 μL of solution at the lowest concentration of 12% w/w) before needle clogging stopped irreversibly the electrospinning process. Fibers in this case appear in the form of isolated strands (2 x $10^3$ fibers per mm) with an average diameter of ~340 nm. As with MEK, fiber continuity is interrupted due to the formation of numerous beads (width of 2-8 μm and length of 5-20 μm) and the surface morphology of the fibers is inhomogeneous. In general, such discontinuities are observed at any solution concentration (Figure S7e).

Using THF, electrospinning was not interrupted by needle clogging, but the produced fibers are, nevertheless, discontinuous with beads and a large variety of surface morphologies. Fibers exhibit an average diameter of ~570 nm, and a density below $1x10^3$ fibers per mm for solutions at 12% polymer/solvent (Figure S7f). Finally in case of MEK beads and surface discontinuity can be strongly reduced but the resulting fibers are still in the form of isolated strands (1x $10^2$ fibers per mm) with an average diameter of 590 nm even after 1 hour of continuous spinning (Figure S7g).

**Supplementary References**

44. Rizvi, M. S., Kumar, P., Katti, D. S. & Pal A. Mathematical model of mechanical behavior of micro/nanofibrous materials designed for extracellular matrix substitutes. *Acta Biomaterialia* **8,** 4111–4122, (2012).